Extreme Mechanics Letters 40 (2020) 100845

Contents lists available at ScienceDirect

Extreme Mechanics Letters

journal homepage: www.elsevier.com/locate/eml

Making something out of nothing: Enhanced flaw tolerance and rupture resistance in elastomer–void "negative" composites

Seunghyun Lee [a,1], Cole D. Fincher [a,1], Russell Rowe [b], Arber Shasivari [a], Edwin Torres [a], Michael Ecker-Randolph [c], Matt Pharr [a,*]

[a] Department of Mechanical Engineering, Texas A&M University, College Station, TX, 77843, United States of America
[b] Department of Mechanical Engineering, Lamar University, Beaumont, TX, 7705, United States of America
[c] Department of Mechanical and Aerospace Engineering, West Virginia University, Morgantown, WV, 26505, United States of America

ARTICLE INFO

Article history:
Received 19 February 2020
Received in revised form 20 May 2020
Accepted 22 June 2020
Available online 24 June 2020

Keywords:
Elastomers
Voids
Fracture
Damage
Composites

ABSTRACT

Elastomers often exhibit large stretchability but are not typically designed with robust energy dissipating mechanisms. As such, many elastomers are sensitive to the presence of flaws: cracks, notches, or any other features that cause inhomogeneous deformation significantly decrease the effective stretchability. To address this issue, we have dispersed voids into a silicone elastomer matrix, thereby creating a "negative" composite that provides increased fracture resistance and stretchability in pre-cut specimens while simultaneously decreasing the weight. Experiments and simulations show that the voids locally weaken the specimen, guiding the crack along a tortuous path that ultimately dissipates more energy. We investigate two geometries in pre-cut specimens (interconnected patterns of voids and randomly distributed discrete voids), each of which more than double the energy dissipated prior to complete rupture, as compared to that of the pristine elastomer. We also demonstrate that the energy dissipated during fracture increases with the volume fraction of the voids. Overall, this work demonstrates that voids can impart increased resistance to rupture in elastomers with flaws. Since additive manufacturing processes can readily introduce/pattern voids, we expect that applications of these elastomer–void "composites" will only increase going forward, as will the need to understand their mechanics.

© 2020 Elsevier Ltd. All rights reserved.

1. Introduction

Imbued with high reversible stretchability, soft elastomers have found a wide range applications from industrial sealing [1–4] and dielectric sensors/transducers [5–9] to biomedical implants [10–12] and soft robotics [13–15]. Of particular note, the elastic compliance and large reversible stretchabilities of silicone-based elastomers render them as ideal candidates for a new generation of flexible, stretchable, and wearable electronics [16–20]. Still, many of these applications require resilience to extreme mechanical loading, including large stretching, bending, and twisting without incurring damage, i.e., they require large fracture resilience. Additionally, large-scale applications have been proposed, e.g., in using dielectric elastomers to harvest energy from ocean waves [21]. In large-scale applications, flaws from the manufacturing process tend to be larger than in producing smaller specimens. Likewise, 3D printing of elastomers is an emerging field but typically produces relatively large flaws during the printing process [22–26]. With sufficiently large flaws or any other features that cause inhomogeneous deformation (e.g., clamped boundary conditions), elastomers are prone to rupture.

To achieve better mechanical performance in these applications, previous research has focused on making stronger and tougher elastomers through chemical modifications (e.g., introducing double networks of crosslinked elastomers) [27,28] and by adding reinforcing materials [29–33]. Notably, previous studies in elastomers have demonstrated the potential of stiff reinforcing materials to improve mechanical performance [32,34]. One well known example of a particle-reinforced composite is carbon black filled rubber [35]. In these systems, interfacial bonding between the particles and matrix, the shape and size of the filler, and the distribution of the particles all affect the mechanical behavior of the composite system [36]. In specific regards to silicone-based elastomers, previous studies have utilized silica particles [37], liquid metals [32], and fibers [31,34] to strengthen the material. From a fracture perspective, some of these studies have demonstrated crack-tip deflection during fracture due to interactions of the cracks with the reinforcing materials [32,34]. The deflection

* Corresponding author.
E-mail address: m-pharr@tamu.edu (M. Pharr).
[1] Denotes equal contribution.

https://doi.org/10.1016/j.eml.2020.100845
2352-4316/© 2020 Elsevier Ltd. All rights reserved.

can produce longer crack paths during rupture or can even temporarily arrest the crack at certain positions, thereby increasing the overall toughness and allowing regions ahead of the crack to sustain more load prior to macroscopic failure [27,32,38]. However, adding reinforcing materials to an elastomeric matrix usually engenders complex fabrication processes, additional cost, and increases in weight. Likewise, most of these composites are comprised of soft matrices and stiff filler; as such, the material stiffness increases, which typically decreases stretchability.

In this work, rather than adding a reinforcing material, we disperse voids into the silicone elastomer matrix, thereby creating a "negative composite". Similar structures are, in fact, commonly used in tissue scaffolding [39–43]. These voids reduce the weight of the specimen, increase the compliance, and intuitively locally weaken the materials. As a result, the voids provide a means of crack-tip deflection, thereby guiding the crack along a more tortuous path and potentially into configurations less susceptible to subsequent propagation. To demonstrate these effects, we perform uniaxial tension tests of pre-cut specimens with two general void geometries (interconnected diamond patterns and randomly-distributed spherical voids) and quantify their fracture resilience relative to that of the base elastomer (and each other). We also perform fracture tests with single extended voids oriented at various angles relative to a pre-cut to provide insight into interactions between cracks and defects. Corresponding finite element simulations elucidate how stress/strain fields evolve as the crack approaches these defects, ultimately producing deflection. Overall, this paper demonstrates that the introduction of voids can increase the effective fracture resistance and stretchability while simultaneously reducing weight in elastomers with flaws.

2. Material and methods

2.1. Architected void specimen preparation

We use an approach similar to that of Mohanty et al. [44] to fabricated architected void specimens. Figure S1 shows the fabrication procedure step-by-step. First, polyvinyl alcohol (PVA) was 3D printed in the desired pattern using eSUN brand 1.75 mm PVA filament (Figure S1a). Smooth-On Ecoflex 00-30 platinum catalyzed silicone elastomer was adopted as the matrix material. When pouring an elastomer mixture over the printed PVA patterns, the PVA print tends to float to the top of the mixture. To ensure that the PVA was located in the center of the parts thickness, we poured the elastomer in two steps. First Parts A and B were mixed in a 1:1 ratio and poured into a mold up to two-thirds of mold thickness (Figure S1b). A printed PVA pattern was submerged in the solution, allowed to float to the top, and then cured at room temperature for 2 h (Figure S1c). We then poured additional elastomer solution into the mold to fill the last third of the mold thickness, as to center the PVA structure through the thickness of the elastomer (Figure S1d). After the elastomer completely cured for 4 h at room temperature, the lateral edges of the resulting specimen were trimmed with a razorblade to expose the PVA. The PVA, a water-soluble material, was then completely dissolved out of the specimen by placing the specimen in circulated water and on a hot plate for 48 h at 80 °C (Figure S1e & S1f).

2.2. Elastomer–bubble composite preparation

We have adopted a similar fabrication method for elastomer–bubble composites to that of Miiriyev et al. [45]. Along with Smooth-On Ecoflex 00–30 Part A and B (1:1 mixing ratio), ethanol (KOPTEC, 200 proof) was mixed in at 1, 5, 10, and 20 percent volume fractions, followed by 24 h of curing in a mold at room temperature. The volume fraction of bubbles generated during the curing time depended upon the volume the mixing ratio of ethanol. Cross-sectional images (seen in Figure S2) enabled the determination of the average bubble diameter and number in a given cross section, which were used in calculating the approximate bubble volume fraction (assuming spherical bubble geometries). 0.2, 8.9, 10.1, and 19.4 bubble volume % were obtained from the 1, 5, 10, and 20 percent volume fractions of ethanol, respectively.

2.3. Specimen geometries

For the fracture tests of the pure elastomer, architected void composites, and elastomer–bubble composites, we implemented a "pure shear" type geometry [46] with a specimen thickness of $t_1 = 4.5$ mm, length $L = 76.2$ mm, and height $H = 25.4$ mm, as labeled in Fig. 1c. For pre-cut specimens, a razor blade produced a 25.4 mm pre-cut at the left edge and mid-plane through the height. The architected void specimens implemented extended rectangular prisms in a diamond pattern with internal angles of 75° and 105°, thickness of voids $t_2 = 2.2$ mm, and width of voids $d = 2$ mm (Fig. 1c). (Fig. 1c). The dimensions of the single void with oblique angles specimens are specimen thickness of $t_1 = 3$ mm, length $L = 152.4$ mm, height $H = 25.4$ mm, and a pre-cut of length 25.4 mm, as shown in Fig. 2.

2.4. Finite element analysis

ABAQUS finite element software was used to simulate specimens with a columnar void as seen in Fig. 3. The dimensions of the model are 25.4 mm × 76.2 mm and 3 mm thickness. The simulations implemented a 20-node quadratic brick, reduced integration, hybrid with linear pressure type element (C3D20RH). The lower face was given a fixed boundary condition. The upper face of the specimen was displaced to produce a stretch of $\lambda = 2$. The material properties were defined through hyperelastic behavior, inputting the stress–strain data from a uniaxial tension test of a pure (no voids) elastomer specimen (no pre-cut) to determine the coefficients for the incompressible Mooney–Rivlin constitutive model ($U = C_{10}\left(\overline{I_1} - 3\right) + C_{01}\left(\overline{I_2} - 3\right)$), which gave $C_{10} = 0.01134$, and $C_{01} = 0.0001766$.

2.5. Mechanical testing

All testing was conducted on an Instron 5943 system using a displacement control loading mode. The specimens were glued into "pure-shear" geometry grips with Loctite gel superglue, and a 25.4 mm pre-cut was made at the mid-plane and left edge of the specimen with a fresh razorblade. Cross-head displacements were measured to calculate the stretch of the samples during testing. The videos indicated minimal slip between the grips and the specimens. The stretch at propagation was determined by time synchronizing the load–displacement and corresponding video footage during the experiments. Both the architected void specimens and the elastomer–bubble composite samples were tested at a stretch rate of 1/min.

3. Results and discussion

3.1. Effects of interconnected architected voids on the fracture behavior of silicone elastomers

We have investigated fracture behavior in a pre-cut silicone elastomer both with and without architected voids. The samples with architected voids consisted of interconnected voids of rectangular prisms in the elastomer (Fig. 1). We designed this void

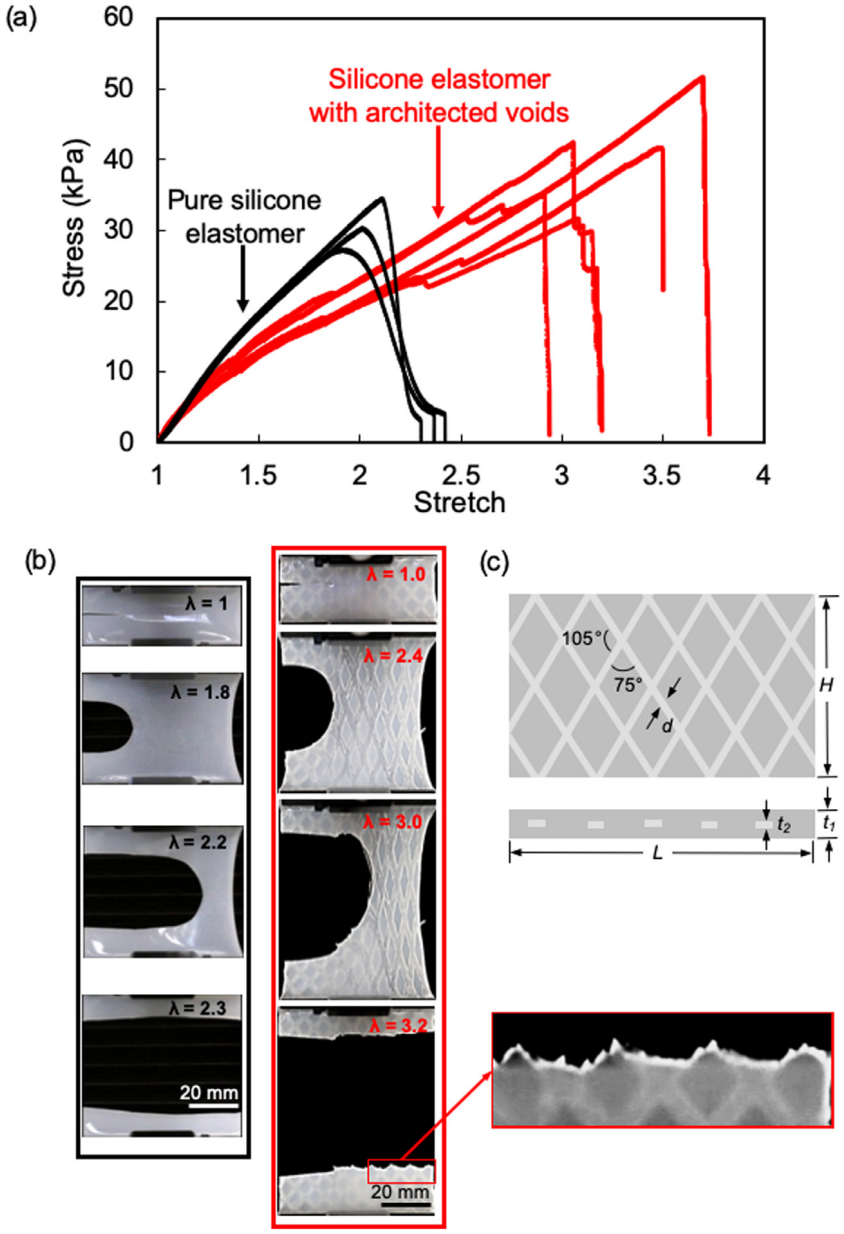

Fig. 1. (a) Stress–stretch curves of a pure silicone elastomer and the same silicone elastomer with architected voids. Each specimen was pre-cut and loaded under uniaxial tension. (b) Corresponding snapshots during fracture testing. $\lambda = 1.8$ is the stretch at the onset of crack propagation in the pure silicone elastomer, and $\lambda = 2.4$ is the stretch at the onset of crack propagation in architected elastomer. Corresponding videos are provided in the supporting information (Videos S1 and S2). (c) Schematics of a silicone elastomer with architected voids.

pattern to deflect and "guide" the crack by generating locally weaker regions in the elastomer. A pre-cut was introduced into the samples prior to loading. Fig. 1 shows the engineering stress–stretch response of pre-cut silicone elastomers (Ecoflex 00-30) with and without architected voids, along with representative photos during crack propagation. We should note that the stress here is the engineering stress, defined as the force at a given time divided by the initial (total external) cross-sectional area, i.e., we do not subtract out any area of the voids or any dimension of the crack. We adopt the "pure shear" geometry of Rivlin and Thomas [46], loaded in the vertical direction using displacement control at a constant stretch rate of 1/min. For the pure (no void) silicone elastomer (black curves in Fig. 1a), the stress increases with increasing stretch until reaching a critical value (31 ± 3.1 kPa occurring at $\lambda = 2.0 \pm 0.1$), at which point the crack begins to propagate straight across the sample, as seen in the second image of the black series in Fig. 1b. A drop in load occurs during crack propagation, as the region behind the crack front has no (or little) load bearing capability. For the pure (no void) elastomers, during crack propagation, the stress decreases with stretch in a smooth and continuous fashion, as seen in Fig. 1a and Video S1.

For the architected void samples, crack propagation initiates at a stress of 22.7 ± 7.24 kPa with a stretch of 2.1 ± 0.4 as seen in Fig. 1a and in the second image of the red series in Fig. 1b. Moreover, in the architected samples, the crack does not propagate forward quickly. Instead, as the crack begins to propagate forward, it turns to deflect along the locally-weaker void pattern (Video S2). In doing so, the crack orients itself more parallel to the loading direction, thereby reducing the stress ahead of the crack (in the "forward" direction). As a result, the strain energy release rate decreases, stopping the crack temporarily, and requiring that the external load increase prior to further propagation. As

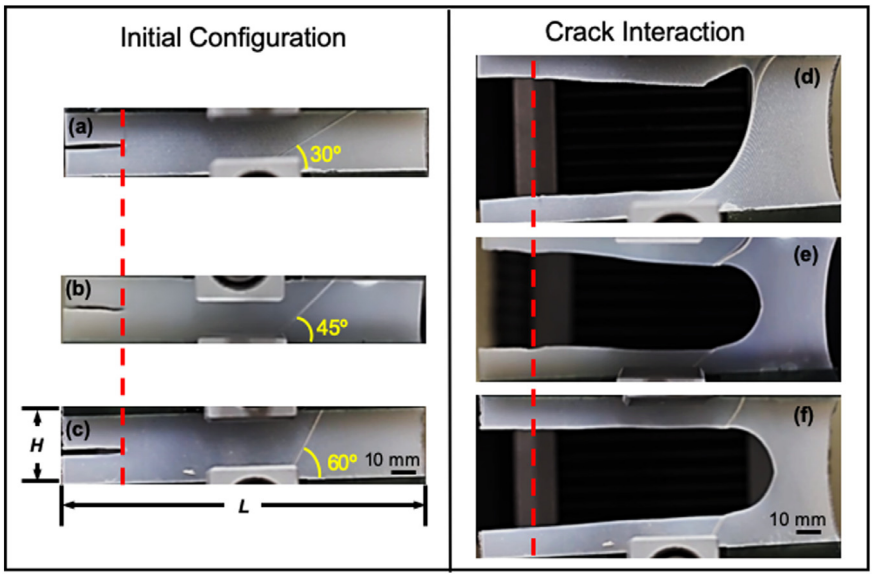

Fig. 2. (a), (b), and (c) represent the initial configuration of precut specimens with single columnar voids initially at (a) 30°, (b) 45°, and (c) 60° to the precut (horizontal). (d), (e), and (f) represent the corresponding images as the crack interacts with the void. Corresponding videos are provided in the supporting information (Videos S3, S4, and S5, respectively).

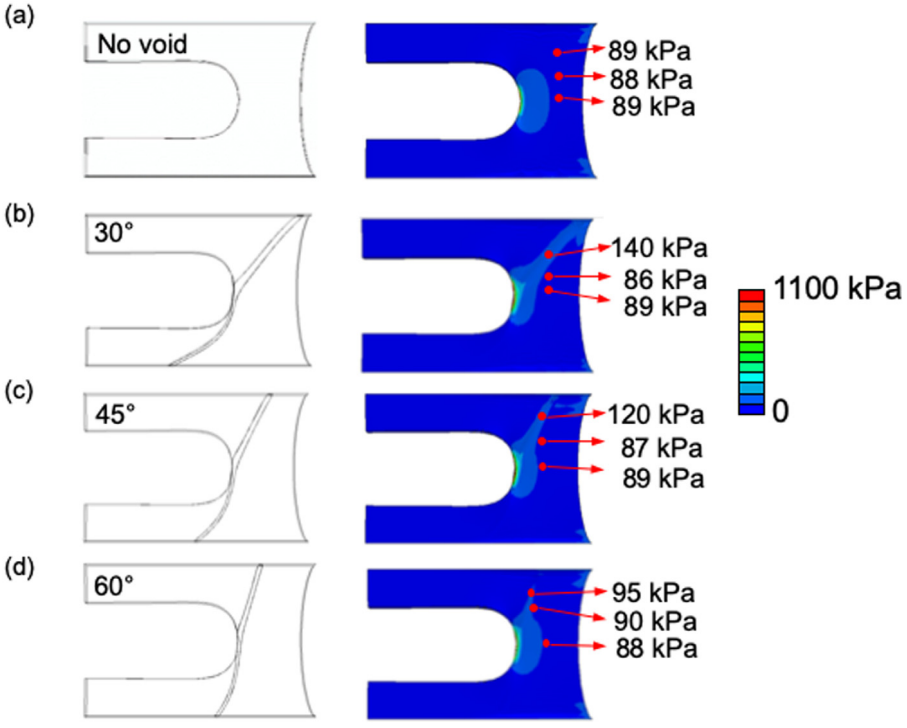

Fig. 3. Deformed geometries and contour plots of the maximum principal stress for (a) a pristine specimen (no void), and for specimens with a single columnar void initially at (b) 30°, (c) 45°, and (d) 60° angles to the pre-cut direction (horizontal). Localized stresses occur near the void but this effect diminishes with increasing angle between the void and the horizontal.

the load increases, the crack continues to propagate intermittently, frequently arresting before switching directions (leading to observable kinks in the stress–stretch curve). Overall, this tortuous path of the crack improves the samples' resistance to complete failure. As calculated by integrating the area under the stress–stretch curve (often referred to as the tensile toughness in materials without a pre-cut), the total energy dissipated by the architected voids specimens is 61.3 ± 12.4 kJ/m^3 for the samples tested. This value is nearly three times the energy dissipated by the pre-cut pure (no void) silicone elastomer samples (23.3 ± 1.4 kJ/m^3). We should note that these values depend on the geometry (e.g., if we used a specimen with a larger length, these values would increase) and here are used for comparative purposes among our various structures.

We conducted additional experiments and ABAQUS simulations to provide further insight into the mechanism governing the crack path. Namely, we performed additional "pure shear" type tests on specimens with a single void at an oblique angle (at 30°, 45°, and 60° to the pre-cut at the beginning of the test), as seen in the left-most column of Fig. 2. Upon reaching a

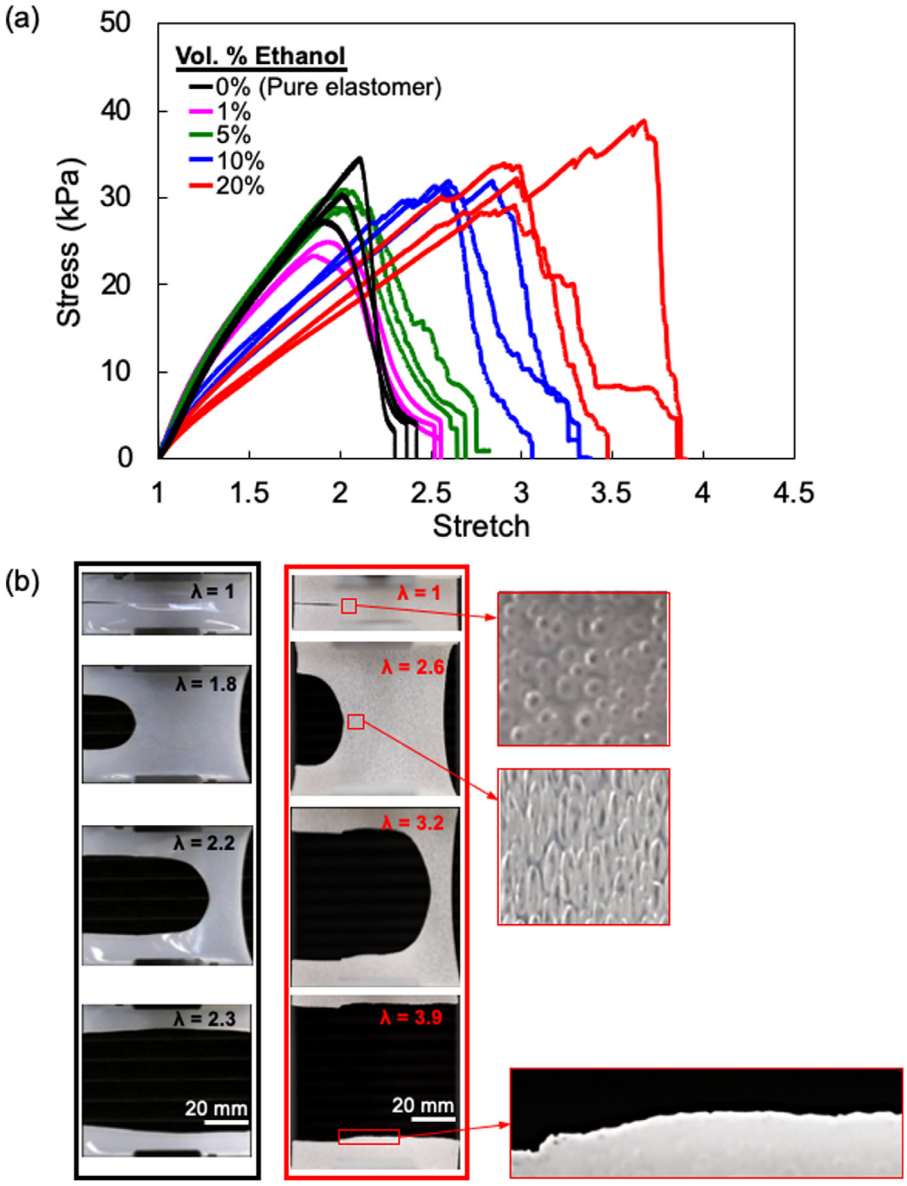

Fig. 4. (a) Stress–stretch curves of pure silicone elastomers and elastomer–bubble composites of different volume ratios. The samples were pre-cut and loaded uniaxial tension. (b) Corresponding snapshots of a pure specimen (no voids) and for 20% ethanol volume fraction. The second images in each column represent the time at which the crack began to propagate, while the bottom images represent the moment just after complete failure.

critical load, the crack began to propagate in the direction of the initial pre-cut. As seen in the right column of Fig. 2, for the 45° and 60° samples, the crack continues to propagate through the defect undeterred. However, for the 30° sample, the crack path clearly follows the angle of the void. Corresponding videos are provided in the supporting information (Videos S3, S4, and S5). This result confirms the intuitive idea that a crack is more likely to follow a void that is closely aligned with the direction perpendicular to the largest component of stress, i.e., at a small angle relative to the pre-cut direction. Fig. 3 displays finite element simulations in ABAQUS that support this intuition by showing the local deformation and stress fields as the crack approaches voids at various angles to the crack. The region in front of the crack appears similar for the pure and the 60° samples. However, for the sample with a void at 30°–45° to the crack, the region near the void and ahead of the crack tip shows a high local stress. As a result, it is easy to see how a thin ligament of material along the void will rupture more readily than will the dense area directly in front of the crack. We should note that these single void studies cannot be directly compared (e.g., in terms of deflection angles) to the architected void specimens due to a number of discrepancies between the two: the architected void samples have higher overall compliance, the effective angle of interaction as the crack tip approaches the void depends on the initial distance between the crack and the void, the stress fields of each void in the architected structures interact, etc. Instead, these single void experiments and corresponding simulations are included to provide insight into the origin of the crack deflection along a void (the stress fields created by the void and crack tip interact to deflect the crack along the locally weaker void). They also demonstrate that in designing such structures, it is important to realize there are limitations (a crack is more likely to follow a void that is closely aligned with the direction perpendicular to the largest component of stress).

These results suggest that the likelihood for the crack to propagate along a void depends on the angle between the crack and direction of maximum principal stress in regions ahead of the crack tip, i.e., the "direction" of the defect relative to the crack. As

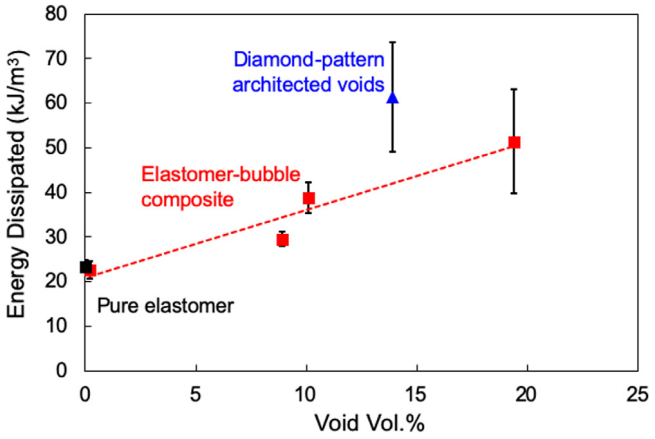

Fig. 5. The energy dissipated by pre-cut specimens versus void volume percent. The energy dissipated was calculated by integrating the area under the stress–stretch curves until the specimen failed completely.

the crack deflects along an angled void, it aligns itself more with the applied load, which decreases the subsequent driving force for crack propagation, thereby potentially arresting the crack. Additionally, with increasing strain, the void further rotates relative to the initial pre-cut direction, which leads the crack to turn to an even higher angle that is even less favorable for propagation. Voids with larger dimensions relative to the thickness of the sample should also increase the likelihood of the crack to follow the void, as the ligament of solid material is thinner, further increasing the stresses in regions near the void.

We also performed experiments to assess whether the matrix material itself affects the ability of voids to deflect cracks. To this end, we performed tests on PDMS polydimethylsiloxane (PDMS), which is stiffer and more brittle than Ecoflex 00-30, with single voids oriented at 30° to the pre-cut. As seen in Fig. 2a and Video S3, the crack readily deflects along the void in Ecoflex 00-30. However, in PDMS (shown in Figure S3), the crack propagates continuously through the specimen, impervious to the void. As such, it is important to note that the effectiveness of "negative composite" structures will certainly depend on the mechanical properties of the matrix material, thereby motivating future studies.

Overall, Figs. 1–3 show that the architected voids have important effects on the mechanical behavior of pre-cut silicone elastomers: (1) The voids weaken the material locally, increasing the favorability for the crack to propagate along the void, i.e., for the crack to deflect, (2) the effective strength and stretchability of pre-cut specimens increases in samples with voids, and (3) the overall energy dissipated during the fracture process increases in samples with voids. We should also mention that crack deflection and hence energy dissipation likely depends on the diameter of the void relative to the thickness of the sample, the spacing between the voids relative to the size of the voids, and the angle between the void and crack. In the scope of this manuscript, we have not attempted to optimize these parameters but these considerations warrant future studies.

3.2. Discontinuous voids and scaling of energy dissipation with void volume fraction

While the experiments in Fig. 1 use interconnected networks of voids, we also investigated discontinuous voids, as seen in Fig. 4. These samples were produced by adding ethanol into the elastomer mixture, which leads to well-distributed bubble formation during curing [36]. Controlling the relative amount of ethanol produced specimens with a similar distribution of bubble diameters (near 0.5 mm, as seen in Figure S2) but with a varied volume fraction of bubbles. The resulting specimen was then stretched at a stretch rate of 1/min. Similar to the architected void samples from Fig. 1, the elastomer–bubble composites in Fig. 4 display a perturbed crack path with intermittent crack propagation (Video S6) but seemingly to a somewhat lesser extent than in the architected void specimens (Video S2). Furthermore, while the crack propagates at similar stress levels in each of the specimens, the stretch at propagation increased with bubble volume fraction, with averages stretches at propagation of 1.79, 1.91, 2.36, and 2.53 for 0.2, 8.9, 10.1, and 19.4 bubble volume %, respectively. Stretches at complete rupture also increased with increasing bubble volume fraction, with averages of 2.54, 2.69, 3.21, and 3.73 for 0.2, 8.9, 10.1, and 19.4 bubble volume %, respectively. Additionally, Fig. 5 shows the total energy dissipation during crack propagation as calculated by the area under the stress–stretch curves. The dissipated energy appears to increase linearly with the volume percent of ethanol. Notably, the 20% volume fraction ethanol possesses an increase in dissipated energy by a factor of ∼2.5 relative to the pure silicone specimens.

Comparing the interconnected architected void samples with the elastomer–bubble composite samples provides insight into the geometric advantages offered by these void morphologies. Fig. 5 displays symbols and error bars representing the average and standard deviation of the energy dissipated for the diamond-pattern architected voids (red series in Fig. 1), as well as the elastomer–bubble composite and the pre-cut pure elastomer samples tested at a 1/min stretch rate. For the architected void samples, the volume occupied by the voids is 13.9% of the total volume. The inset in Fig. 1b shows the failure surface (side view) for a representative architected void sample, while the inset in the bottom right image of Fig. 4b shows a failure surface (side view) for a elastomer–bubble composite sample. As seen in Fig. 5, the architected void dissipates more energy than does the elastomer–bubble composite for the same volume fraction. This difference likely stems from the path that the crack follows for in each geometry. In the architected void samples, the crack is forced to follow a long path, occasionally kinking or switching direction when given the chance to propagate in a direction more aligned with the normal to the loading direction (as happens in the middle of the "X" in the patterned structure). Meanwhile, the crack deflections in the elastomer–bubble composites are much smaller due to the presence of many small bubbles, which provide more opportunities for the crack to travel in a direction more aligned with the normal to the loading direction. Since the crack path can more readily align with the normal to the loading direction, the stress component acting perpendicular to the path is larger for the elastomer–bubble composite, which causes the crack to propagate more readily under the same remote load, as compared to the architected voids. As a result, randomly distributed pores and voids in silicone elastomers, as seen in some previous applications [43,45,47], provide general improvement in energy dissipation for parts with flaws. However, geometries with extended defects, à la interconnected extended voids, may possess increased energy dissipation as compared to random voids: the extended defects "trick" the crack into following a longer and more tortuous path and even frequently leading to the crack getting "stuck" along the way (e.g., as in Video S2). However, given that the crack's ability to deflect depends upon the angle between the void and the network (as indicated in Figs. 2–3), more work should be conducted to confirm that the architected void networks at various angles still continue to dissipate more energy than the discrete voids (elastomer–bubble composite).

We note that the presence of voids and inclusions has previously been shown to decrease the strength of dogbone specimens

of elastomers [25]. In addressing this possibility, we tested dog-bone specimens (without pre-cuts) for the pristine elastomer, as well as the elastomer–bubble composite and the architected elastomer samples (Figure S4). Indeed, the sample fails earlier in both the architected and elastomer–bubble composite samples, as compared to the pure elastomer, a finding consistent with previous studies. Thus, while the incorporation of voids may help improve the mechanical performance of flawed specimens, they do not necessarily improve the performance of specimens without flaws. However, we argue that while many parts used in practice do not have pre-cuts per se, many do have cracks, notches, or other features causing inhomogeneous deformation that act as flaws. For instance, the "flaw" may in fact be a rigid electronic component bonded to the elastomer, a sudden change in geometry along the loading direction, or a sharp change in material type within a composite specimen. Thus, "negative composites" may prove useful for mitigating failure in such applications.

4. Conclusions

Fracture resilience is a key characteristic in developing effective elastomer components in applications. While conventional composites employ hard and stiff inclusions to improve mechanical properties, we find that the opposite approach (introducing infinitely-compliant voids) leads to improvements in mechanical performance in "flawed" silicone elastomers, i.e., specimens with cracks, notches, or any other features that cause inhomogeneous deformation. Specifically, we demonstrate that voids introduced into pre-cut silicone elastomer specimens locally "weaken" the specimen, which intriguingly enhances its overall resistance to rupture. We detail two methods of introducing voids (producing extended interconnected architected voids and discrete spherical bubbles) that disrupt crack propagation, thereby increasing the effective strength, stretchability, and energy dissipation during fracture of pre-cut specimens. We also establish that the resistance to rupture (in terms of total energy dissipation) appears to scale linearly with the volume fraction of discontinuous voids. Our findings also suggest that the fracture resilience depends on void shape/connectivity and the mechanical properties of matrix material. Future work may further optimize the geometry and composition of negative composites towards enhanced energy dissipation and fracture resistance in elastomers.

Declaration of competing interest

The authors declare that they have no known competing financial interests or personal relationships that could have appeared to influence the work reported in this paper.

Acknowledgments

S.L. and C.D.F. contributed equally to this work. C.D.F. acknowledges the support of the National Science Foundation Graduate Research Fellowship, United States under grant No. 1746932. M.P. and S.L. acknowledge funding from the mechanical engineering department at Texas A&M University, United States and the Texas A&M Engineering Experimentation Station (TEES), United States. R.R. and M.E.R. were funded through NSF REU site, United States Grant # EEC 1757882.

Appendix A. Supplementary data

Supplementary material related to this article can be found online at https://doi.org/10.1016/j.eml.2020.100845.

References

[1] J.K. Whanger, S.J. Harrall, Reinforced swelling elastomer seal element on expandable tubular. (Google Patents), 2004.
[2] D.D. Brown, Expansion joint with elastomer seal. (Google patents), 1977.
[3] Y. Lou, A. Robisson, S. Cai, Z. Suo, Swellable elastomers under constraint, J. Appl. Phys. 112 (3) (2012) 034906.
[4] Z. Wang, C. Chen, Q. Liu, Y. Lou, Z. Suo, Extrusion, slide, and rupture of an elastomeric seal, J. Mech. Phys. Solids 99 (2017) 289–303.
[5] H. Zhang, M.Y. Wang, J. Li, J. Zhu, A soft compressive sensor using dielectric elastomers, Smart Mater. Struct. 25 (3) (2016) 035045.
[6] Z. Xu, S. Zheng, X. Wu, Z. Liu, R. Bao, W. Yang, M. Yang, High actuated performance MWCNT/Ecoflex dielectric elastomer actuators based on layer-by-layer structure, Composites A 125 (2019) 105527.
[7] Q. Wang, Z. Suo, X. Zhao, Bursting drops in solid dielectrics caused by high voltages, Nature Commun. 3 (1157) (2012).
[8] D. Kwon, T.-I. Lee, J. Shim, S. Ryu, M.S. Kim, S. Kim, T.-S. Kim, I. Park, Highly sensitive, flexible, and wearable pressure sensor based on a giant piezocapacitive effect of three-dimensional microporous elastomeric dielectric layer, ACS Appl. Mater. Interfaces 8 (26) (2016) 16922–16931.
[9] O. Atalay, A. Atalay, J. Gafford, C. Walsh, A highly sensitive capacitive-based soft pressure sensor based on a conductive fabric and a microporous dielectric layer, Adv. Mater. Technol. 3 (1) (2018) 1700237.
[10] J. Courtney, T. Gilchrist, Silicone rubber and natural rubber as biomaterials, Med. Biol. Eng. Comput. 18 (4) (1980) 538–540.
[11] K.Y. Lee, D.J. Mooney, Hydrogels for tissue engineering, Chem. Rev. 101 (7) (2001) 1869–1880.
[12] J.J. Marler, J. Upton, R. Langer, J.P. Vacanti, Transplantation of cells in matrices for tissue regeneration, Adv. Drug Deliv. Rev. 33 (1–2) (1998) 165–182.
[13] R. Pelrine, R. Kornbluh, Q. Pei, J. Joseph, High-speed electrically actuated elastomers with strain greater than 100%, Science 2875454 (2000) 836–839.
[14] D. Yang, B. Mosadegh, A. Ainla, B. Lee, F. Khashai, Z. Suo, K. Bertoldi, G.M. Whitesides, Buckling of elastomeric beams enables actuation of soft machines, Adv. Mater. 27 (41) (2015) 6323–6327.
[15] I.A. Anderson, T.A. Gisby, T.G. McKay, B.M. O'Brien, E.P. Calius, Multi-functional dielectric elastomer artificial muscles for soft and smart machines, J. Appl. Phys. 112 (4) (2012) 041101.
[16] Y. Liu, M. Pharr, G.A. Salvatore, Lab-on-skin: a review of flexible and stretchable electronics for wearable health monitoring, ACS Nano 11 (10) (2017) 9614–9635.
[17] D.-H. Kim, N. Lu, R. Ma, Y.-S. Kim, R.-H. Kim, S. Wang, J. Wu, S.M. Won, H. Tao, A. Islam, Epidermal electronics, Science 3336044 (2011) 838–843.
[18] M. Amjadi, Y.J. Yoon, I. Park, Ultra-stretchable and skin-mountable strain sensors using carbon nanotubes–Ecoflex nanocomposites, Nanotechnology 26 (37) (2015) 375501.
[19] Y. Ma, M. Pharr, L. Wang, J. Kim, Y. Liu, Y. Xue, R. Ning, X. Wang, H.U. Chung, X. Feng, Soft elastomers with ionic liquid-filled cavities as strain isolating substrates for wearable electronics, Small 13 (9) (2017) 1602954.
[20] S. Yao, Y. Zhu, Wearable multifunctional sensors using printed stretchable conductors made of silver nanowires, Nanoscale 6 (4) (2014) 2345–2352.
[21] R. Pelrine, R.D. Kornbluh, J. Eckerle, P. Jeuck, S. Oh, Q. Pei, S. Stanford, Dielectric elastomers: generator mode fundamentals and applications, in: Smart Structures and Materials 2001: Electroactive Polymer Actuators and Devices, (International Society for Optics and Photonics), 2001, pp. 148–156.
[22] J. Herzberger, J.M. Sirrine, C.B. Williams, T.E. Long, Polymer design for 3D Printing Elastomers: Recent advances in structure, properties, and printing, Prog. Polym. Sci. (2019) 101144.
[23] J. Rossiter, P. Walters, B. Stoimenov, Printing 3D dielectric elastomer actuators for soft robotics, in: Electroactive Polymer Actuators and Devices (EAPAD) 2009, (International Society for Optics and Photonics), 2009, p. 72870H.
[24] D.K. Patel, A.H. Sakhaei, M. Layani, B. Zhang, Q. Ge, S. Magdassi, Highly stretchable and UV curable elastomers for digital light processing based 3D printing, Adv. Mater. 29 (15) (2017) 1606000.
[25] J. Plott, X. Tian, A.J. Shih, Voids and tensile properties in extrusion-based additive manufacturing of moisture-cured silicone elastomer, Addit. Manuf. 22 (2018) 606–617.
[26] J.P. Moore, C.B. Williams, Fatigue characterization of 3D printed elastomer material, in: 19th Annual International Solid Freeform Fabrication Symposium (SFF), Austin, TX, Aug, 2008, pp. 4–6.
[27] R. Bai, J. Yang, X.P. Morelle, Z. Suo, Flaw-Insensitive Hydrogels under static and Cyclic loads, Macromol. Rapid Commun. 40 (8) (2019) 1800883.
[28] J. Wu, L.H. Cai, D.A. Weitz, Tough self-Healing Elastomers by Molecular Enforced integration of Covalent and reversible networks, Adv. Mater. 29 (38) (2017) 1702616.
[29] W.R. Illeperuma, J.-Y. Sun, Z. Suo, J.J. Vlassak, Fiber-reinforced tough hydrogels, Extreme Mech. Lett. 1 (2014) 90–96.

[30] S. Lin, C. Cao, Q. Wang, M. Gonzalez, J.E. Dolbow, X. Zhao, Design of stiff, tough and stretchy hydrogel composites via nanoscale hybrid crosslinking and macroscale fiber reinforcement, Soft Matter 10 (38) (2014) 7519–7527.
[31] Q. He, Z. Wang, Y. Yan, J. Zheng, S. Cai, Polymer nanofiber reinforced double network gel composite: Strong, tough and transparent, Extreme Mech. Lett. 9 (2016) 165–170.
[32] N. Kazem, M.D. Bartlett, C. Majidi, Extreme toughening of soft materials with liquid metal, Adv. Mater. 30 (22) (2018) 1706594.
[33] W.-C. Lin, W. Fan, A. Marcellan, D. Hourdet, C. Creton, Large strain and fracture properties of poly (dimethylacrylamide)/silica hybrid hydrogels, Macromolecules 43 (5) (2010) 2554–2563.
[34] Z. Wang, C. Xiang, X. Yao, P. Le Floch, J. Mendez, Z. Suo, Stretchable materials of high toughness and low hysteresis, Proc. Natl. Acad. Sci. 116 (13) (2019) 5967–5972.
[35] G. Hamed, B. Park, The mechanism of carbon black reinforcement of SBR and NR vulcanizates, Rubber Chem. Technol. 72 (5) (1999) 946–959.
[36] S. Ahmed, F. Jones, A review of particulate reinforcement theories for polymer composites, J. Mater. Sci. 25 (12) (1990) 4933–4942.
[37] L. Bokobza, Elastomeric composites. I. Silicone composites, J. Appl. Polym. Sci. 93 (5) (2004) 2095–2104.
[38] S. Lee, M. Pharr, Sideways and stable crack propagation in a silicone elastomer, Proc. Natl. Acad. Sci. 116 (19) (2019) 9251–9256.
[39] S. Sarkar, M. Dadhania, P. Rourke, T.A. Desai, J.Y. Wong, Vascular tissue engineering: microtextured scaffold templates to control organization of vascular smooth muscle cells and extracellular matrix, Acta Biomater. 1 (1) (2005) 93–100.
[40] S.J. Hollister, Porous scaffold design for tissue engineering, Nature Mater. 4 (7) (2005) 518.
[41] Y. Mi, Y. Chan, D. Trau, P. Huang, E. Chen, Micromolding of PDMS scaffolds and microwells for tissue culture and cell patterning: A new method of microfabrication by the self-assembled micropatterns of diblock copolymer micelles, Polymer 47 (14) (2006) 5124–5130.
[42] S. Pilla, Handbook of Bioplastics and Biocomposites Engineering Applications, John Wiley & Sons, 2011.
[43] D.J. Mooney, D.F. Baldwin, N.P. Suh, J.P. Vacanti, R. Langer, Novel approach to fabricate porous sponges of poly (D, L-lactic-co-glycolic acid) without the use of organic solvents, Biomaterials 17 (14) (1996) 1417–1422.
[44] S. Mohanty, L.B. Larsen, J. Trifol, P. Szabo, H.V.R. Burri, C. Canali, M. Dufva, J. Emnéus, A. Wolff, Fabrication of scalable and structured tissue engineering scaffolds using water dissolvable sacrificial 3D printed moulds, Mater. Sci. Eng. C 55 (2015) 569–578.
[45] A. Miriyev, K. Stack, H. Lipson, Soft material for soft actuators, Nature Commun. 8 (1) (2017) 596.
[46] R. Rivlin, A.G. Thomas, Rupture of rubber. I. Characteristic energy for tearing, J. Polym. Sci. 10 (3) (1953) 291–318.
[47] Y. Li, D. Zhu, S. Handschuh-Wang, G. Lv, J. Wang, T. Li, C. Chen, C. He, J. Zhang, Y. Liu, Bioinspired, mechano-regulated interfaces for rationally designed, dynamically controlled collection of oil spills from water, Glob. Chall. 1 (3) (2017) 1600014.